

An Assumed Strain Triangular Solid Element for Efficient Analysis of Plates and Shells with Finite Rotation

J. H. Kim¹, Y. H. Kim¹, and S. W. Lee²

Abstract: A simple triangular solid shell element formulation is developed for efficient analysis of plates and shells undergoing finite rotations. The kinematics of the present solid shell element formulation is purely vectorial with only three translational degrees of freedom per node. Accordingly, the kinematics of deformation is free of the limitation of small angle increments, and thus the formulation allows large load increments in the analysis of finite rotation. An assumed strain field is carefully selected to alleviate the locking effect without triggering undesirable spurious kinematic modes. In addition, the curved surface of shell structures is modeled with flat facet elements to obviate the membrane locking effect. Various numerical examples demonstrate the efficiency and accuracy of the present element formulation for the analysis of plates and shells undergoing finite rotation. The present formulation is attractive in that only three points are needed for numerical integration over an element.

keyword: Triangular solid shell element, assumed strain formulation, finite rotations

1 Introduction

In the last two decades, a substantial number of formulations have been presented to improve the performance of the finite elements designed for analysis of plate and shell structures. These elements can be classified by their planar geometry into two types: triangular elements and quadrilateral elements. As far as the modeling of arbitrary geometry is concerned, the triangular elements are more advantageous than the quadrilateral elements because of the conveniences in local mesh refinement and automatic mesh generation [Peraire, Vahdati, Morgan, and Zienkiewicz (1987), Nambiar, Valera, and Lawrence (1993)].

However, the triangular elements, as well as the quadrilateral elements, suffer from the locking effect that severely deteriorates the computational performance of the finite element models unless appropriate remedies are implemented. To construct triangular element models free of the locking effect, numerous approaches have been investigated and reported. For example, the discrete Kirchhoff plate theory [Sze, Zhu, and Chen (1997), Murthy and Gallagher (1986)], the flat facet triangular element concept [Allman (1994)], the stabilization matrix method [Fish and Belytschko (1992), Cook (1993)] and the assumed strain formulation [Kim, Kim and Lee (2000)] have been proposed to reduce the locking effect of the triangular element in the linear analysis of plates and shells.

Since the finite element method evolved, many researchers have had great concerns on the efficient analysis when dealing with the structures with finite rotations. Recently, a bunch of studies presented some improvements on the analysis of the finite rotation of beams [Beda (2003), Ijima, Obiwa, Iguchi and Goto (2003), Iura, Suetake, and Atluri (2003), Lin and Hsiao (2003), Okamoto and Omura (2003), Zupan and Saje (2003), Ibrahimbegovic and Knopf-Lenoir (2003), Goutou, Kuwataka, Nishihara and Iwakuma (2003)] and shells [Basar AND Kintzel (2003), Briseghella, Majorana, and Pavan (2003), Suetake, Iura, Atluri (2003)].

The finite element formulations involving triangular elements also have been applied to the analysis of plates and shells undergoing finite rotation. More recent studies can be found in the works by Onate, Zarate, and Flores (1994), Poulsen and Damkilde (1996) and Keulen and Booij (1996) among others. Onate, Zarate, and Flores (1994) have developed a triangular element with six rotational degrees of freedom (DOF) at mid-side nodes. Poulsen and Damkilde (1996) proposed a flat triangular shell element with rotational DOF at loop nodes. In addition, Keulen and Booij (1996) constructed a 12-DOF

¹ SNU, Seoul, Republic of Korea

² University of Maryland, MA, U.S.A

flat facet triangular element in which mid-side rotation is replaced with relative rotation. These elements show fairly high accuracy in the analysis of geometrically nonlinear behavior of plates and shells. However, the conventional shell elements involving rotational DOF often require too many load steps due to their innate assumption of small angle increments. As demonstrated by Lee and his associates [Kim and Lee (1988), Park, Cho, and Lee (1995)] with a quadrilateral element, this shortcoming can be overcome through the solid shell element approach. In this approach shells are treated as a three-dimensional solid and a solid element tailored for shell analysis is constructed, based on the assumed strain formulation. As an alternate approach that allows thickness change, Simo, Fox, and Rifai (1990) introduced a shell element formulation with stretchable directors through thickness.

In the present paper, a simple triangular solid shell element formulation is developed for analysis of shells undergoing finite rotation. For this, the 36-DOF triangular solid shell element presented in Reference 7 for linear analysis is extended to geometrically nonlinear analysis. The curved shell geometry is modeled with flat facet triangles to obviate the membrane locking effect [Allman (1994), Poulsen and Damkilde (1996), Stolarski and Belytschko (1983)]. By adopting the kinematics of the solid element approach, the present triangular element formulation is expected to allow load increments much larger than is possible for the conventional shell formulation with the rotational parameters. The finite element formulation is based on the assumed strain approach in which an independently assumed strain field is introduced to reduce the locking effect without triggering detrimental spurious kinematic modes [Kim, Kim, and Lee (2000), Lee and Pian (1978)].

Numerical tests with various examples undergoing finite rotations are conducted to demonstrate the efficiency and accuracy of the present triangular solid shell element.

2 Finite element formulation

2.1 Triangular solid element configuration and kinematics

Fig. 1 shows the present 12-node triangular solid element with six nodes on both top and bottom surfaces. Each node has only three translational DOF, resulting in an element with 36 DOF. The difference of the displacement

vectors between top and bottom surface nodes can be related to the rotations around the inplane vectors on the midsurface. Alternatively, through the use of proper kinematic relationship, the element can be transformed into a six node with six DOF per node.

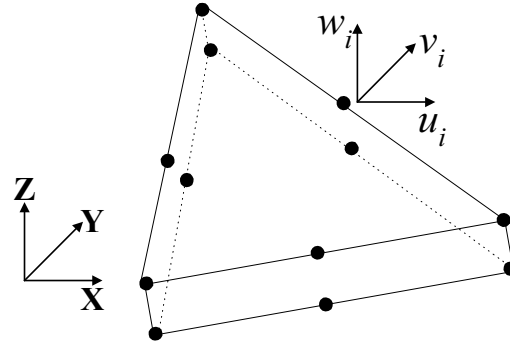


Figure 1 : Twelve node triangular solid element, 3DOF/node

2.2 Equilibrium equation and compatibility equation

For a solid in equilibrium, the virtual work is expressed in integral form as follows:

$$\int (\delta \bar{\mathbf{E}})^T \mathbf{S} dV - \delta W = 0 \quad (1)$$

In equation (1), $\delta \bar{\mathbf{E}}$ is the virtual strain vector, \mathbf{S} is the second Piola-Kirchhoff stress vector, δW is the virtual work done due to external load. Superscript T stands for vector or matrix transpose, and the integration is performed over the volume of the undeformed configuration. Introducing the independently assumed strain vector \mathbf{E} , the compatibility equation is expressed in integral form as follows:

$$\int (\delta \mathbf{S})^T (\bar{\mathbf{E}} - \mathbf{E}) dV = 0 \quad (2)$$

The stress-strain relationships for elastic material is expressed such that:

$$\mathbf{S} = \mathbf{C} \mathbf{E} \quad (3)$$

where \mathbf{C} is the 6x6 elastic constitutive matrix. To be consistent with the kinematics of shell deformation, the

constitutive matrix is reformed such that there is no coupling between the inplane normal strains and the transverse normal stress [Kim, Kim, and Lee (2000), Kim and Lee (1988)].

Substituting equation (3) into equations (1) and (2), the equilibrium and compatibility equation can be expressed in terms of displacement-dependent strain vector and independently assumed strain vector as follows:

$$\int (\delta \bar{\mathbf{E}})^T \mathbf{C} \mathbf{E} dV - \delta W = 0 \quad (4)$$

$$\int (\delta \mathbf{E})^T \mathbf{C} (\bar{\mathbf{E}} - \mathbf{E}) dV = 0 \quad (5)$$

For iterative solution techniques in nonlinear analysis, the nodal degrees of freedom vector \mathbf{q}_e are expressed in incremental form as follows:

$$\mathbf{q}_e = {}^k \mathbf{q}_e + \mathbf{D} \mathbf{q}_e \quad (6)$$

where ${}^k \mathbf{q}_e$ represents the resulting nodal degrees of freedom vector after the k-th iteration, $\mathbf{D} \mathbf{q}_e$ is incremental nodal degrees of freedom vector at current iteration, and the variables with subscript e indicate the elemental quantities. Then, the displacement-dependent strain vector is expressed as

$$\bar{\mathbf{E}} = {}^k \bar{\mathbf{E}} + \mathbf{D} \bar{\boldsymbol{\varepsilon}} + \mathbf{D} \bar{\boldsymbol{\eta}} \quad (7)$$

where ${}^k \bar{\mathbf{E}}$ is the resulting strain vector obtained after the k-th iteration, $\mathbf{D} \bar{\boldsymbol{\varepsilon}}$ and $\mathbf{D} \bar{\boldsymbol{\eta}}$ represent the strain vectors that are linear and nonlinear in incremental displacement, respectively. For the linearized iteration of the Newton-Raphson method, $\mathbf{D} \bar{\boldsymbol{\eta}}$ is neglected hereafter.

Similarly, the virtual strain vector is expressed as:

$$\delta \bar{\mathbf{E}} = \delta \bar{\boldsymbol{\varepsilon}} + \delta \bar{\boldsymbol{\eta}} \quad (8)$$

The independently assumed strain vector in incremental form and its virtual vector are expressed as follows:

$$\mathbf{E} = {}^k \mathbf{E} + \mathbf{D} \boldsymbol{\varepsilon} \quad (9)$$

$$\delta \mathbf{E} = \delta \boldsymbol{\varepsilon} \quad (10)$$

Substituting Eqs. (7-9) into Eq. (4) and neglecting high order terms, the equilibrium equation can be reformed as

$$\begin{aligned} & \sum_e \int \left[\delta \bar{\boldsymbol{\varepsilon}}^T \mathbf{C} \mathbf{D} \boldsymbol{\varepsilon} + \delta \bar{\boldsymbol{\eta}}^T \mathbf{C} {}^k \mathbf{E} + \delta \bar{\boldsymbol{\varepsilon}}^T \mathbf{C} {}^k \mathbf{E} \right] dV \\ & = \sum_e \delta W_e \end{aligned} \quad (11)$$

where the notation \sum with subscript e stands for summation over elements.

Similarly, using Eqs. (7), (9), (10) and neglecting high order terms, Eq. (5) of compatibility condition can be expressed as follows:

$$\begin{aligned} & \sum_e \int \left[\delta \boldsymbol{\varepsilon}^T \mathbf{C} ({}^k \bar{\mathbf{E}} - {}^k \mathbf{E}) \right] dV \\ & + \sum_e \int \left[\delta \boldsymbol{\varepsilon}^T \mathbf{C} \mathbf{D} \bar{\boldsymbol{\varepsilon}} \right] dV - \sum_e \int \left[\delta \boldsymbol{\varepsilon}^T \mathbf{C} \mathbf{D} \boldsymbol{\varepsilon} \right] dV = 0 \end{aligned} \quad (12)$$

Using nodal interpolation function, the incremental strain vector can be symbolically expressed as

$$\mathbf{D} \bar{\boldsymbol{\varepsilon}} = \mathbf{B} \mathbf{D} \mathbf{q}_e \quad (13)$$

where \mathbf{B} is a 6x36 matrix relating the strain vector to the nodal displacement vector. In a similar manner, the virtual strain vectors, $\delta \bar{\boldsymbol{\varepsilon}}$ and $\delta \bar{\boldsymbol{\eta}}$, are expressed as:

$$\delta \bar{\boldsymbol{\varepsilon}} = \mathbf{B} \delta \mathbf{q}_e \quad (14)$$

$$\delta \bar{\boldsymbol{\eta}} = \delta \mathbf{q}_e \mathbf{R} \mathbf{D} \mathbf{q}_e \quad (15)$$

where $\delta \mathbf{q}_e$ is the virtual nodal degree of freedom vector, and the matrix \mathbf{R} is obtained from the nonlinear strain-displacement relations.

The incremental assumed strain vector $\mathbf{D} \boldsymbol{\varepsilon}$ and the virtual strain vector $\delta \boldsymbol{\varepsilon}$ can be expressed as:

$$\mathbf{D} \boldsymbol{\varepsilon} = \mathbf{P} \mathbf{D} \boldsymbol{\alpha} \quad (16)$$

$$\delta \boldsymbol{\varepsilon} = \mathbf{P} \delta \boldsymbol{\alpha} \quad (17)$$

where $\mathbf{P}(\xi, \eta, \zeta)$ is the assumed strain interpolation matrix defined in parent coordinate system and $\boldsymbol{\alpha}$ is the assumed strain parameter vector.

Substituting equations (13), (16), (17) into equation (12) leads to the following relation:

$$\Delta \boldsymbol{\alpha} = \mathbf{H}^{-1} \mathbf{G} \mathbf{D} \mathbf{q}_e + \mathbf{H}^{-1} F \quad (18)$$

where

$$\mathbf{F} = \int \mathbf{P}^T \mathbf{C} ({}^k \bar{\mathbf{E}} - {}^k \mathbf{E}) dV \quad (19)$$

$$\mathbf{G} = \int \mathbf{P}^T \mathbf{C} \mathbf{B} dV \quad (20)$$

$$\mathbf{H} = \int \mathbf{P}^T \mathbf{C} \mathbf{P} dV \quad (21)$$

Using equations (14-16) and (18), equation (11) for the linearized equilibrium equation becomes

$$\sum_e \delta \mathbf{q}_e^T (\mathbf{K}_e \mathbf{D} \mathbf{q}_e - \mathbf{D} \mathbf{Q}_e) = 0 \quad (22)$$

where the stiffness matrix and load vector at element level is

$$\mathbf{K}_e = \mathbf{G}^T \mathbf{H}^{-1} \mathbf{G} + \mathbf{K}_S \quad (23)$$

$$\mathbf{D} \mathbf{Q}_e = \mathbf{Q}_a - \mathbf{G}^T \mathbf{H}^{-1} \mathbf{F} - {}^k \mathbf{Q} \quad (24)$$

The initial stress stiffness matrix \mathbf{K}_S is constructed based on the current stress obtained after the k -th iteration. The initial stress load vector ${}^k \mathbf{Q}$ and the external load vector \mathbf{Q}_a are defined as

$${}^k \mathbf{Q} = \int \mathbf{B}^T \mathbf{C}^k \mathbf{E} dV \quad (25)$$

$$\delta W_e = \delta \mathbf{q}_e^T \mathbf{Q}_a \quad (26)$$

After assembling over all elements, equation (22) becomes

$$\mathbf{K} \mathbf{D} \mathbf{q} = \mathbf{D} \mathbf{Q} \quad (27)$$

which can be solved for $\mathbf{D} \mathbf{q}$.

3 Assumed strain

3.1 Assumed strain field

In the present formulation the assumed strain fields are tailored to alleviate the locking effect while maintaining kinematic stability. In order to reduce locking, the assumed strain field must be chosen as simple as possible. However, an oversimplified strain field may trigger detrimental spurious kinematic modes. The assumed strain field chosen for the present investigation is as follows [Kim, Kim and Lee (2000)]:

$$\begin{aligned} E_{xx} &= \alpha_1 + \alpha_2 \xi + \alpha_3 \eta + \zeta (\alpha_4 + \alpha_5 \xi + \alpha_6 \eta) \\ E_{yy} &= \alpha_7 + \alpha_8 \xi + \alpha_9 \eta + \zeta (\alpha_{10} + \alpha_{11} \xi + \alpha_{12} \eta) \\ E_{zz} &= \alpha_{13} + \alpha_{14} \xi + \alpha_{15} \eta \\ E_{xy} &= \alpha_{16} + \alpha_{17} \xi + \alpha_{18} \eta + \zeta (\alpha_{19} + \alpha_{20} \xi + \alpha_{21} \eta) \\ E_{yz} &= \alpha_{22} + \alpha_{23} \xi + \alpha_{24} \eta + \zeta (\alpha_{15} + \alpha_{25} \xi + \alpha_{26} \eta) \\ E_{zx} &= \alpha_{27} + \alpha_{24} \xi + \alpha_{23} \eta + \zeta (\alpha_{14} + \alpha_{28} \xi + \alpha_{25} \eta) \end{aligned} \quad (28)$$

In equation (28) ξ , η , and ζ are the parent coordinates with ξ , η embedded in the triangular plane and ζ normal to the plane.

Note that the transverse shear strain fields are chosen such that they share common coefficients among themselves and with the transverse normal strain field. The assumed strain fields in equation (28) can be expressed in matrix form as

$$\mathbf{E} = \mathbf{P} \boldsymbol{\alpha} \quad (29)$$

Incremental form of equation (29) appears in equation (16).

3.2 Numerical integration rule

Based on the assumed strain field as well as the displacement field, the present study adopts three-point rule for numerical integration over the midsurface with the sampling points located at (1/6, 2/3), (1/6, 1/6) and (2/3, 1/6) in the parent coordinate system for a triangle. Integration through thickness is carried out analytically, following the approach used by Kim and Lee (1988).

3.3 Local coordinate system and element invariance

In the present formulation, the assumed transverse shear strain fields are composed of incomplete polynomial terms. As a result, the element stiffness matrix varies with the coordinate system in which strain and stress components are defined. Accordingly, a specifically defined local coordinate system is needed to enforce the invariance of the element stiffness. The local coordinate system used in the present study is shown in Fig. 2. First, the largest angle in a triangle is bisected. Then the x and y axes of the local coordinate system are defined over the shell mid-plane 45 degrees off from the bisecting line. The z axis is normal to the plane defined by the x and y axes. This local coordinate system is defined for each element to ensure the element invariance.

3.4 Spurious kinematic modes and kinematic stability

It turns out that, for geometrically linear case, the assumed strain field defined in equation (28) triggers two spurious kinematic modes. For a triangular element with right angle and two equal side lengths, the spurious kinematic modes are found as follows:

$$u = \rho xy, \quad v = -\rho xy \quad (30)$$

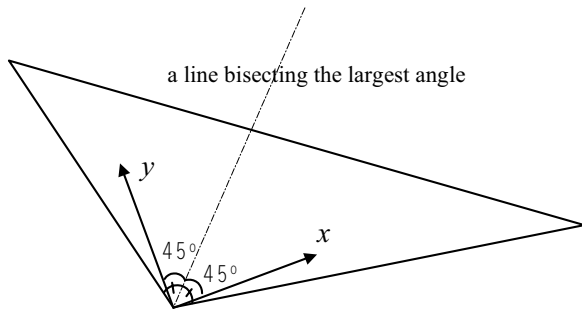


Figure 2 : A local coordinate system defined for each element

$$w = \gamma(x^2 - y^2) \quad (31)$$

where ρ , γ are arbitrary constants. These modes are identified by applying the zero strain energy condition at the sampling points of numerical integration in an element. However, they are incompatible spurious kinematic modes and thus disappear when four or more elements are assembled, resulting in a stable global stiffness matrix with sufficient ranks. Also, it can be shown by following Park, Cho, and Lee. (1995) that, for geometrically nonlinear case, the above two modes disappear even at element level and the element is completely free of any spurious kinematic modes.

4 Numerical tests

In order to validate the performance of the present assumed strain triangular element, numerical tests are carried out for several plate and shell examples undergoing geometrically nonlinear deformation. For geometrically nonlinear analysis, the Newton-Raphson iteration method is used. The arc-length method with the minimum residual displacement [Chan (1988)] is used for the analysis beyond the limit point. Of particular interest is the ability of the present formulation to allow large load increment in finite rotation problems. In the following, numerical results obtained by the present formulation are labeled ‘Present’. They are compared with the results, labeled ‘Reduced’, obtained by the assumed displacement formulation with reduced integration using the three-point rule.

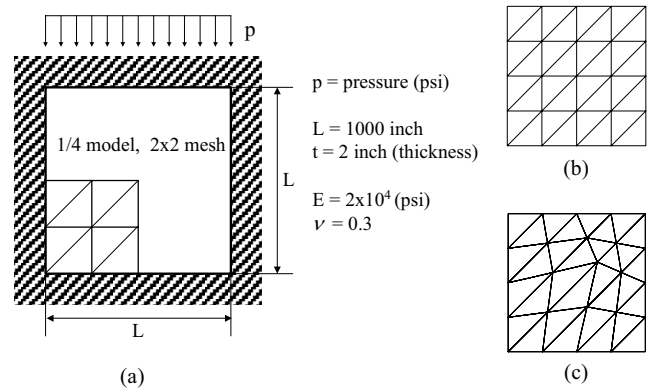


Figure 3 : (a) Clamped square plate under uniform pressure; (b) 4x4 uniform mesh; (c) 4x4 distorted mesh

4.1 Clamped square plate under uniform pressure

A clamped square plate is subjected to uniform pressure as shown in Fig. 3-(a). The side length and the thickness of the plate are $L=1000$ inch and $t=2$ inch, respectively. Elastic material properties are Young’s modulus $E=20000$ psi and Poisson’s ratio $\nu=0.3$. Due to the symmetry of the geometry and loading condition, only a quarter of the plate is discretized with a uniform mesh or a distorted mesh as shown in Fig. 3-(b),(c). The maximum transverse displacement at the center of the plate is evaluated for the increasing pressure load. The numerical solutions obtained by the present study are compared with the analytic solution given by Way (1938) as shown in Fig. 4. The pressure load and the transverse displacement in the figure are normalized by Young’s modulus and thickness of the plate, respectively. The results of the present element show good agreement with Way’s solution even with 3x3 coarse mesh discretization. Mesh distortion sensitivity of the present formulation appears not to be severe as shown in Fig. 4-(b).

4.2 Clamped shallow circular arch under point load

Fig. 5 describes a clamped shallow circular arch subjected to point load at the center of the arch. The dimension of the arch is $R=2.54$ inch, $t=0.0508$ inch and the half angle $\theta=0.707$ radians. The elastic material properties of the arch are $E=6.895 \times 10^{10}$ psi and $\nu=0.25$. Only a half of the arch is modeled with the flat triangular element due to the symmetry of the geometry and the loading condition. The arch experiences symmetric buckling as the concentrated loading increases. The arc length

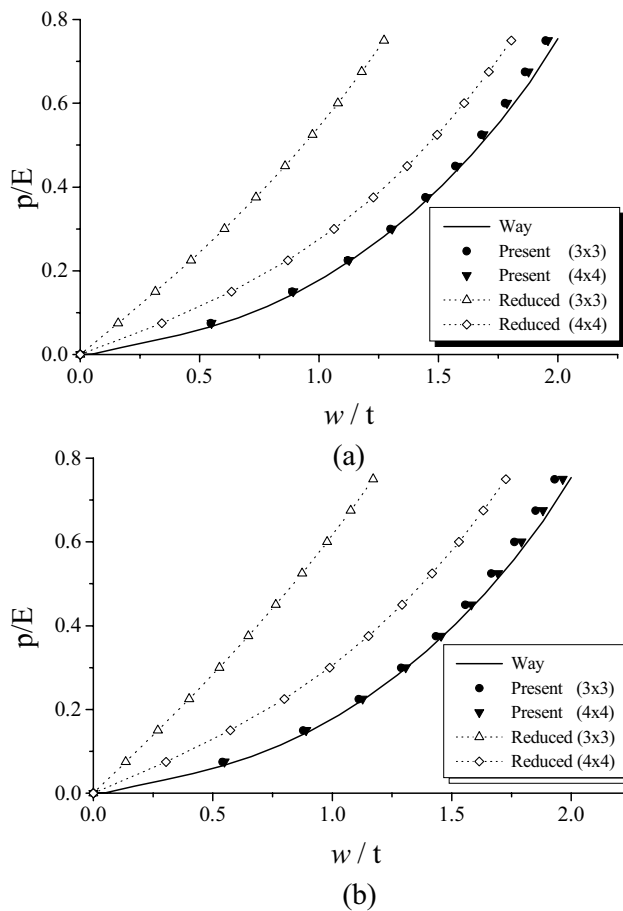


Figure 4 : Normalized transverse displacement at the center of plate; (a) uniform mesh; (b) distorted mesh

method is used for the analysis beyond the limit point. Fig. 6 clearly demonstrates that the present formulation shows good convergent characteristics even beyond the limit point.

4.3 Pinched cylinder with free edges

Fig. 7 shows a cylinder with free edges subjected to normal point loads at two opposite sides. Two loading cases, tension and compression, are tested for the example. The geometric parameters of the cylinder are $R=4.953$ inch, $L=10.35$ inch, and $t=0.094$ inch. Elastic material properties of the cylinder are $E=10.5 \times 10^6$ psi and $\nu=0.3125$. Taking advantage of the symmetry of the geometry and the loading condition, only an octant of the cylinder is modeled with 8×6 uniform mesh of the flat triangular element as shown in Fig. 7. The deformed cross sections of the cylinder for tension and compression loads are as

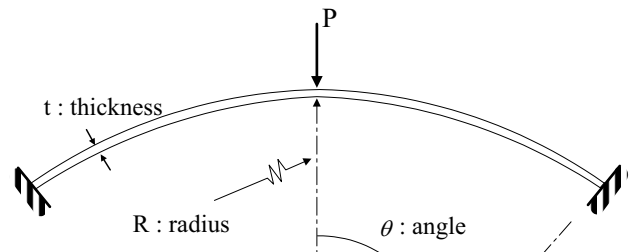


Figure 5 : Clamped shallow circular arch subjected to a point load at the center of the arch

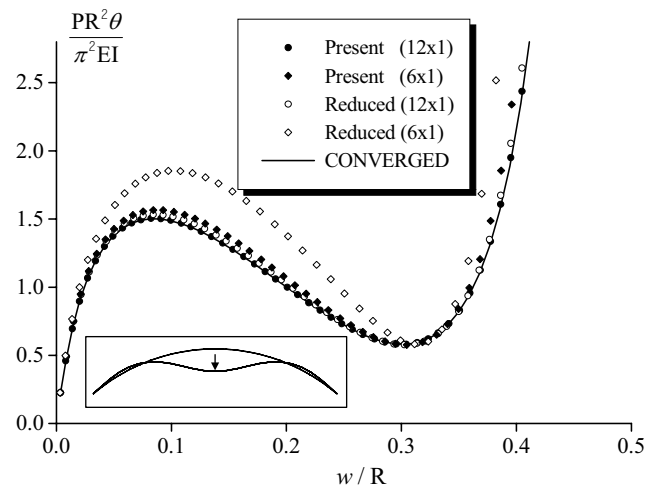


Figure 6 : Normalized transverse displacement of shallow circular arch at the loading point

shown in Fig. 8-(a). The radial displacement at the loading point for the increasing load is shown in Fig. 8-(b) corresponding to ten loading steps or single loading step. The result of the present element agrees well with the analytic solution given by Gruttmann (1989). It is notable that the present solid element model is able to reach the final solution in single load step and to yield the identical result to that obtained by using ten load steps as shown in Fig. 8-(b).

4.4 Cantilever beam subjected to tip roll-up moment

An initially straight beam is subjected to tip roll-up moment as shown in Fig. 9. The roll-up moment is applied by a couple with two forces of equal magnitude at top and bottom surface. The magnitude of roll-up mo-

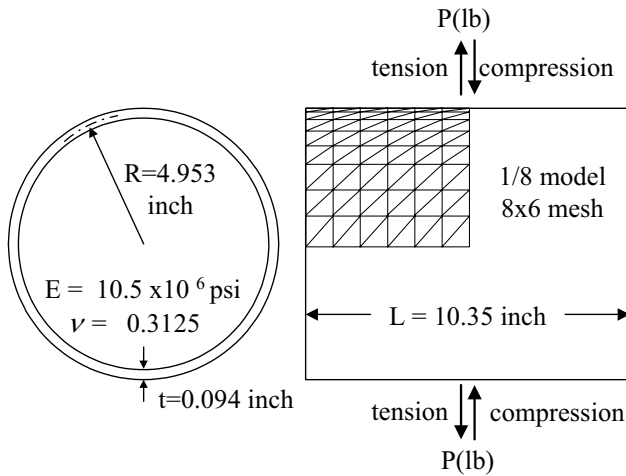


Figure 7 : Pinched cylinder with free edges

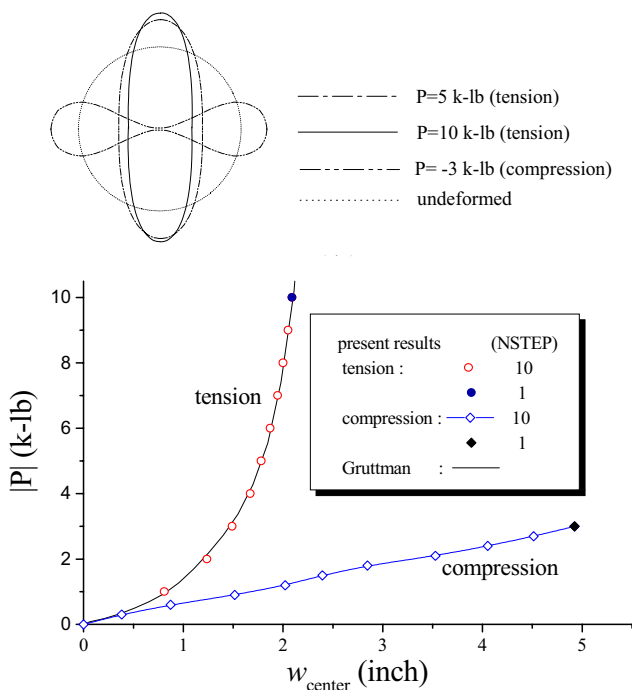


Figure 8 : (a) Deformed cross section of cylinder for tension or compression load; (b) Radial displacement at the loading point using ten loading steps or single loading step

ment and geometrical and material parameters are given in Reference [Buechter and Ramm (1992)]. The dimensions of the beam are such that the side length is 100, the thickness is 2, and the width is 2. The material properties of the beam are $E=21000$ and $\nu=0.0$. The half width of the beam is modeled uniformly with 18×1 mesh. Fig. 9 also show deformed configurations at various tip rotational angles. Each of these configurations is obtained using a single load step. The number of iterations needed to achieve convergence is shown for each configuration. The 360° roll-up of the clamped beam is completed in a single load step with 13 iterations. It is clear that the present element formulation allows large load increments for analysis involving finite rotation.

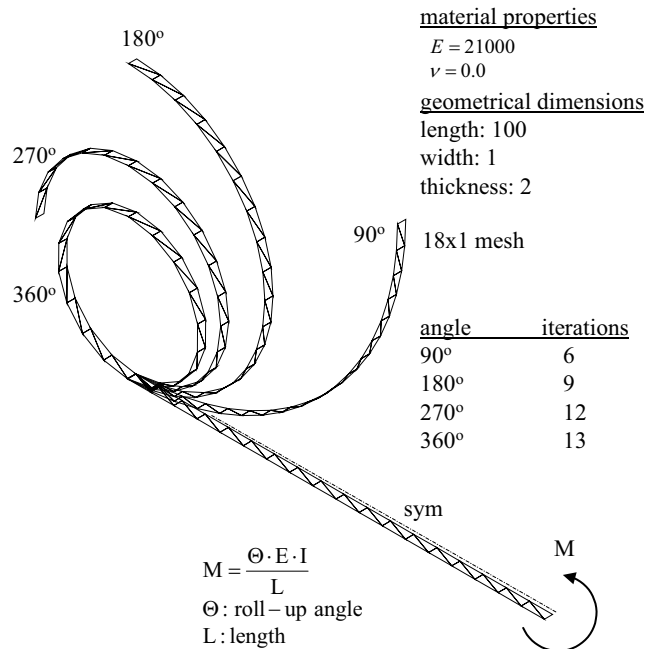


Figure 9 : Cantilever beam subjected to tip roll-up moment

4.5 Cut-out hemisphere under alternating pinched loads

A quarter of a hemisphere with 18° cut-out is modeled with 32×26 flat triangular mesh as shown in Fig. 10. The geometric parameters are radius $R=10$ inch and thickness $t=0.04$ inch. The material properties are $E=6.825 \times 10^7$ and $\nu=0.3$. Both lower and upper boundaries of the hemisphere are free and two alternating point loads are applied

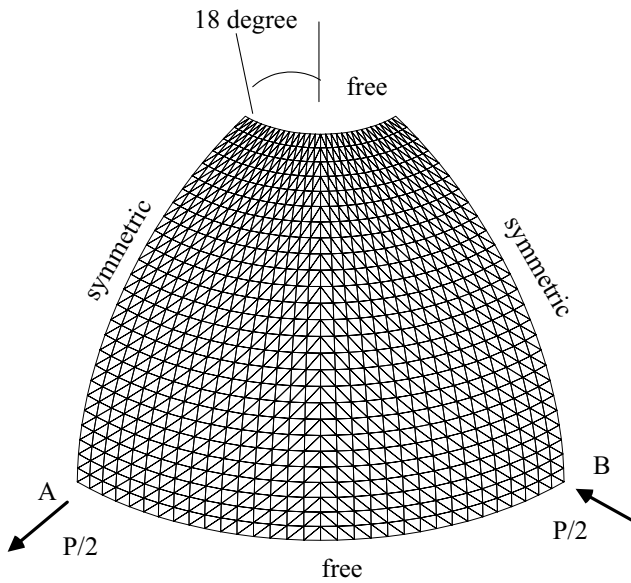


Figure 10 : A quarter of cut out hemisphere subjected to two symmetrical alternating loads

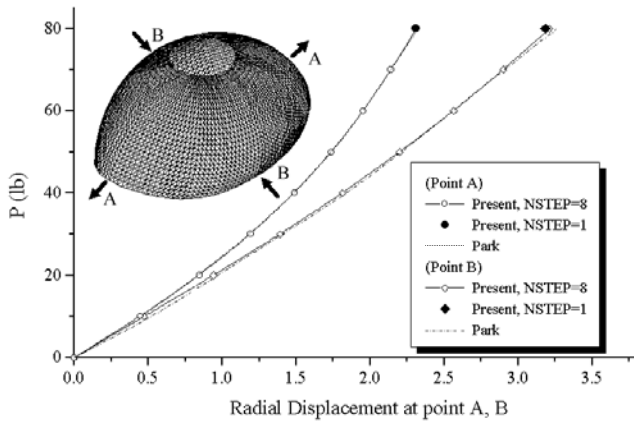


Figure 11 : Radial displacement at two loading points

symmetrically at point A and point B as shown in Fig. 10. With single load step, converged solution for load P of 80 lb is achieved. Fig. 11 demonstrates the present result shows good agreement with the result of Park, Cho, and Lee (1995).

4.6 Sliced ring plate under line load at the free edge

A sliced ring plate is illustrated in Fig. 12-(a). One edge is clamped, and the other edge is free. An upward line load is applied along the free edge. The dimensions of the plate are such that inner radius R_1 is 6 m, outer radius R_2

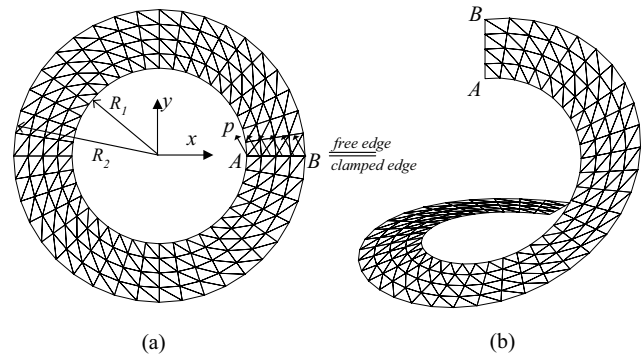


Figure 12 : (a) Sliced ring plate applied by line load along free edge; (b) Deformed shape of ring plate after applying line load $p=4.034$ (N/m)

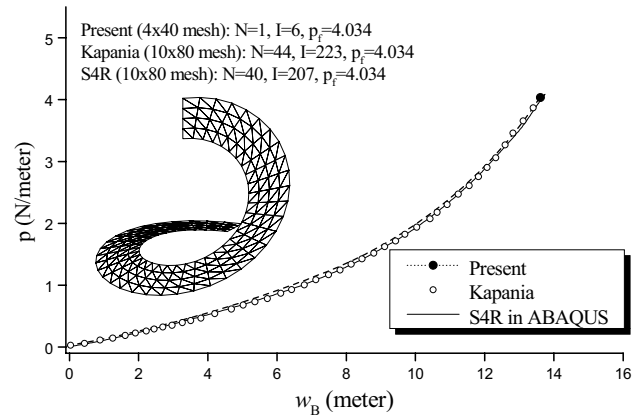


Figure 13 : Maximum disp. vs. load magnitude; N = number of load steps, I = total number of iterations, and p_f = final line load magnitude (N/meter)

is 10 m, and thickness is 0.03 m. The material properties are $E = 2.1 \times 10^8 \text{ N/m}^2$ and $\nu = 0$.

Fig. 12-(b) depicts the deformed shape of the ring plate subjected to line load $p=4.034 \text{ N/m}$ where the final displacement at point B in the loading direction is 13.61 m. The displacement at point B versus the line load magnitude p is plotted in Fig. 13. In addition to the present solution, the results reported by Mohan and Kapania (1998) are included for comparison. Both results show good agreement with each other. However, for the present analysis, same result is efficiently obtained using single load step and six iterations.

4.7 Deep arch with asymmetrical boundary conditions

Fig. 14 shows a deep arch subjected to central load. The end of the arch is clamped and the other is simply supported. The angle of the structure is 215 degree and the thickness is unit. The width is set to be 12 for reasonable aspect ration and the Young’s modulus of material is 10^6 , thus the bending rigidity is 10^6 same with equivalent beam problem [Wood and Zienkiewicz (1977)]. The Poisson ratio is set to be zero to minimize the deformation along width. The structure is modeled with 40 by 1 triangular elements.

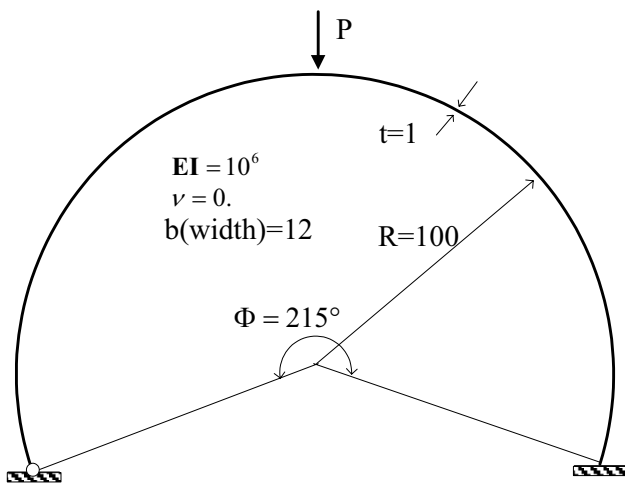


Figure 14 : Deep arch with asymmetric boundary condition subjected to central point load

The deep arch example is introduced to evaluate the present element’s capability of calculating buckling load. Fig. 15 shows the vertical displacement associate with load magnitude compared with analytic solution [Deppo and Schmidt (1975)]. Ibrahimbegovic and Frey (1993) show almost exact overlap with analytic solution using quadratic shear flexible beam element. Fig. 15 demonstrates that the present element shows quite good accuracy for the deep arch problem.

5 Conclusion

A triangular element model with 36 DOF is developed based on the assumed formulation for efficient analysis of plates and shells undergoing finite rotation. The main

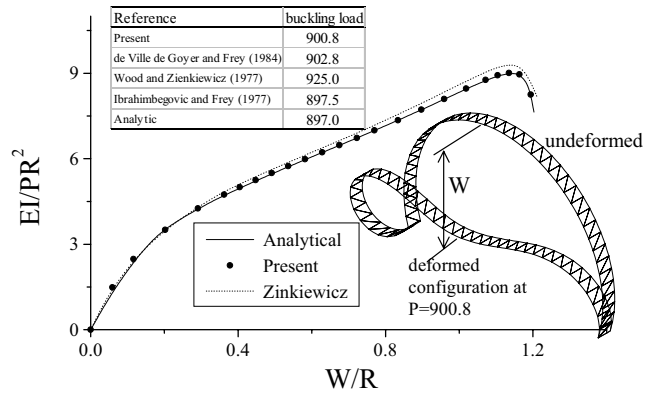


Figure 15 : Buckling load and vertical deflection with respect to the magnitude of load

focus of the present study is to develop a simple triangular shell element that allows large load increments in the geometrically nonlinear analysis. For this, plates and shells are treated as a three-dimensional solid with purely vectorial description of the kinematics of deformation. The assumed strain is carefully selected to alleviate the shear locking effect without triggering undesirable spurious kinematic modes, while the flat facet element concept is adopted to obviate the membrane locking. For geometrically nonlinear plates and shells the present formulation leads to kinematically stable finite element models completely free of any spurious modes. The result of numerical tests validates the accuracy and efficiency of the present formulation within the context of the flat facet element approach. The present triangular element allows large load increments in the analysis of finite rotation, and it is attractive in that only three points are needed for numerical integration.

Acknowledgement: This research was supported in part by a grant from the BK-21 program for Mechanical and Aerospace Engineering Research at Seoul National University. The authors also gratefully acknowledged the financial support from the Ministry of Science and Technology through the National Laboratory Programs

References

Allman, D. J. (1994): A basic flat facet finite elements for analysis of general shells. *Int. j. numer. methods, eng.*. vol. 37, pp.19-36

- Basar, Y.; Kintzel, O.** (2003): Finite Rotations and large Strains in Finite Element Shell Analysis. *CMES: Computer Modeling in Engineering & Sciences*, Vol. 4, No. 2, pp. 217-230
- Beda, P.** (2003): On Deformation of an Euler-Bernolli Beam Under Terminal Force and Couple. *CMES: Computer Modeling in Engineering & Sciences*, Vol. 4, No. 2, pp. 231-238
- Briseghella, L.; Pava, P.** (2003): A Conservative Time Integration Scheme for Dynamics of Elasto-damaged Thin Shells. *CMES: Computer Modeling in Engineering & Sciences*, Vol. 4, No. 2, pp. 273-286
- Buechter, N.; Ramm, E.** (1992): Shell theory versus degeneration-A comparison in large rotation finite element analysis. *Int. j. numer. methods, eng.* vol. 34, pp. 39-59.
- Chan, S. L.** (1988): Geometric and material non-linear analysis of beam-columns and frames using the minimum residual displacement method. *Int. j. numer. methods, eng.* vol. 26, pp. 2657-2669
- Cook, R. D.** (1993): Further development of a three-node triangular shell element. *Int. j. numer. methods, eng.* vol. 36, pp. 1413-1425
- Da Deppo, D. A.; Schmidt, R.** (1975): Instability of clamped-hinged circular arches subjected to a point load. *Trans. Am. Soc. Mech. Eng.*, pp. 894-896
- de Ville de Goyet, V.; Frey, F.** (1984): Use of Marguerre theory in the nonlinear analysis of beams and plate structures. *Proc. 4th world congress on finite element method.* pp. 513-522
- Fish, J.; Belytschko, T.** (1992): Stabilized Rapidly convergent 18-degrees-of-freedom flat shell triangular element. *Int. j. numer. methods, eng.* vol. 33, pp. 149-162
- Gotou, H.; Kuwataka, T.; Nishihara, T.; Iwakuma, T.** (2003): Finite Displacement Analysis Using Rotational Degrees of Freedom about Three Right-angled Axes. *CMES: Computer Modeling in Engineering & Sciences*, Vol. 4, No. 2, pp. 319-328
- Gruttmann, F.; Stein, E.; Wriggers, P.** (1989): Theory and numerics of thin elastic shells with finite rotations. *Ing.-Archiv.* Vol. 59, pp. 54-67
- Ibrahimbegovic, A.; Frey, F.** (1993): Finite element analysis of linear and non-linear planar deformations of elastic initially curved beams. *Int. j. numer. methods, eng.* vol. 36, pp. 3239-3258
- Ibrahimbegovic, A.; Knopf-Lenoir, C.** (2003): Shape Optimization of Elastic Structural Systems Undergoing Large Rotations: Simultaneous Solution Procedure. *CMES: Computer Modeling in Engineering & Sciences*, Vol. 4, No. 2, pp. 337-344
- Ijima, K.; Obiya, H.; Iguchi, S.; Goto, S.** (2003): Element Coordinates and the Utility in Large Displacement Analysis of a Space Frame. *CMES: Computer Modeling in Engineering & Sciences*, Vol. 4, No. 2, pp. 239-248
- Iura, M.; Suetake, Y.; Atluri, S. N.** (2003): Accuracy of Co-rotational Formulation for 3-D Timoshenko's Beam. *CMES: Computer Modeling in Engineering & Sciences*, Vol. 4, No. 2, pp. 249-258
- Keulen, F. V.; Booij, J.** (1996): Refined consistent formulation of a curved triangular finite rotation shell element. *Int. j. numer. methods, eng.* vol. 39, pp. 2803-2820
- Kim, J. H.; Kim, Y. H.; Lee, S. W.** (2000): An assumed strain formulation of efficient solid triangular element for general shell analysis. *Int. j. numer. methods, eng.* vol. 47, pp.1481-1497
- Kim, Y. H.; Lee, S. W.** (1988): A solid element formulation for large deflection analysis of composite shell structures. *Comput. & Struct.* Vol. 30, pp. 269-274
- Lee, S. W.; Pian, T. H. H.** (1978): Improvements of plate and shell finite elements by mixed formulations. *AIAA journal* vol. 16, no.1, pp. 29-34
- Lin, W. Y.; Hsiao, K. M.** (2003): A Buckling and Post-buckling Analysis of Rods Under End Torque and Compressive Load. *CMES: Computer Modeling in Engineering & Sciences*, Vol. 4, No. 2, pp. 259-272
- Mohan, P.; Kapania, R. K.** (1998): Updated Lagrangian Formulation of a Flat Triangular Element for Thin Laminated Shells. *AIAA journal*, vol. 36, no.2, pp. 273-281
- Murthy, S. S.; Gallagher, R. H.** (1986): A triangular thin-shell finite element based on discrete Kirchhoff theory. *Comput. Methods Appl. Mech. Eng.* vol. 54, pp.197-222.
- Nambiar, R. V.; Valera, R. S.; Lawrence, K. L.** (1993): An algorithm for adaptive refinement of triangular element meshes. *Int. j. numer. methods, eng.* vol. 36, pp. 499-509
- Okamoto, S.; Omura, Y.** (2003): Finite-Element Non-linear Dynamics of Flexible Structures in Three Dimen-

sions. *CMES: Computer Modeling in Engineering & Sciences*, Vol. 4, No. 2, pp. 287-300

Onate, E.; Zarate, F.; Flores, F. (1994): A simple triangular element for thick and thin plate and shell analysis. *Int. j. numer. methods, eng.* vol. 37, pp. 2569-2582

Park, H. C.; Cho, C.; Lee, S. W. (1995): An efficient assumed strain element model with six dof per node for geometrically non-linear shells. *Int. j. numer. methods, eng.* vol. 38, pp. 4101-4122

Peraire, J.; Vahdati, M.; Morgan, K.; Zienkiewicz, O. C. (1987): Adaptive remeshing for compressive flow computations. *J. Comp. Phys.*, Vol. 72, pp. 449-466

Poulsen, P. N.; Damkilde, L. D. (1996): A flat triangular shell element with loof nodes. *Int. j. numer. methods, eng.*, vol. 39, pp. 3867-3887

Simo, J. C.; Fox, D. D.; Rifai M. S. (1990): On a stress resultant geometrically exact shell model. Part III: Computational aspects of the nonlinear theory. *Comput. Methods Appl. Mech. Eng.*, vol. 79, pp. 21-76.

Simo, J. C.; Fox, D. D.; Rifai M. S. (1990): On a stress resultant geometrically exact shell model. Part VI: Variable thickness shells with through-the-thickness stretching. *Comput. Methods Appl. Mech. Eng.*, vol. 81, pp. 91-126.

Stolarski, H.; Belytschko, T. (1983): Shear and membrane locking in curved *Co* element. *Comput. meths. appl. mech. enrg.* Vol. 41, pp. 279-296

Suetake, Y.; Iura, M.; Atluri, S. N. (2003): Variational Formulation and Symmetric Tangent Operator for Shells with Finite Rotation Field. *CMES: Computer Modeling in Engineering & Sciences*, Vol. 4, No. 2, pp. 329-336

Sze, K. Y.; Zhu, D.; Chen, D. P. (1997): Quadratic triangular c-zero plate bending element. *Int. j. numer. methods, eng.* vol. 40, pp. 937-951

Way, S. (1938): Uniformly Loaded, Clamped Rectangular Plates with Large Deformation. *Proc. 5th Int. Cong. of Appl. Mech.*, Cambridge, MA

Wood, R. D.; Zienkiewicz, O. C. (1977): Geometrically non-linear finite element analysis of beams-frames-circles and axis-symmetric shells, *Computers and Structures*, vol. 7, pp. 725-735

Zupan, D.; Saje, M. (2003): A new finite element formulation of three-dimensional beam theory based on interpolation of curvature. *CMES: Computer Modeling in Engineering & Sciences*, Vol. 4, No. 2, pp. 301-318

